Liquid Water: When Hyperpolarizability Fluctuations Boost and Reshape the Second Harmonic Scattering Intensities

Guillaume Le Breton, Oriane Bonhomme, Emmanuel Benichou, Claire Loison

Liquid Water : When Hyperpolarizability Fluctuations Boost and Reshape the Second Harmonic Scattering Intensities

Guillaume Le Breton,[†,‡] Oriane Bonhomme,[†] Emmanuel Benichou,[†] and Claire Loison[*,†]

†*Univ Lyon, Univ Claude Bernard Lyon1, CNRS, Light and Matter Institute, F-69622 Villeurbanne, France*

‡*Current address: Department of Chemistry, University of Zurich, CH-8057 Zurich, Switzerland*

E-mail: claire.loison@univ-lyon1.fr

Abstract

Second Harmonic Scattering (SHS) is a method of choice to investigate the molecular structure of liquids. While a clear interpretation of SHS intensity exists for diluted solutions of dyes, the scattering due to solvents remains difficult to interpret quantitatively. Here, we report a quantum mechanics/molecular mechanics (QM/MM) approach to model the polarization-resolved SHS intensity of liquid water, quantifying different contributions to the signal. We point out that the molecular hyperpolarizability fluctuations and correlations cannot be neglected. The intermolecular orientational and hyperpolarizability correlations up to the third solvation layer strongly increase the scattering intensities, and modulate the polarization-resolved oscillation that is predicted here by QM/MM without fitting parameters. Our approach can be generalized to other pure liquids to provide a quantitative interpretation of SHS intensities in terms of short-range molecular ordering.

TOC Graphic

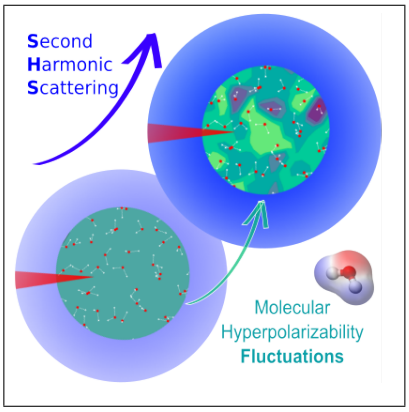

Keywords

Liquid, Water, Nonlinear Optics, Second Harmonic Scattering, Quantum Chemistry, QM/MM, DFT, Optical response, Hyperpolarizability

The molecular structure of liquids is of utmost importance in many phenomena, for example solvation,[1] or flows in ultra confined environments.[2] In particular, liquid water is the subject of numerous studies, because of its importance in everyday life, and in industrial and biological applications. More fundamentally, its specific behaviors are due to subtle interplays between Van der Waals, hydrogen bonding and dipole/dipole forces, leading to both short- and long-range molecular orderings.

Among other experimental techniques, such as Nuclear Magnetic, Resonance,[3] IR-spectroscopies,[4] X-rays or neutrons scattering,[5] Second Harmonic Scattering (SHS) is a method of choice to investigate the molecular structure of liquids. The contribution of orientational correlations in SHS intensities has been known for decades,[6–10] and has recently found renewed interest in probing the molecular structure of various liquids such as organic solvents,[11] ionic liquids,[12] surfactants solutions,[13,14] and salted or pure water.[10,15–17] In particular, for water, the impact of orientational correlations on the second harmonic intensity has been investigated, underlining the importance of both short and long-range structuration.[18–23] The effects induced by interfaces or nano-objects have also been explored.[24–27] However, a quantitative interpretation of all contributions is still missing.

The frameworks developed to investigate orientational correlations from SHS data[7,18,23] are often based on the assumption that all the molecules of the system have the same second harmonic response i.e. the same first hyperpolarizability tensor β. Using this hypothesis, long-range orientation correlations can be extracted from experimental intensities resolved in polarization.[23] Alternatively, if the orientational correlations are known, for example from numerical simulations, an effective hyperpolarizability tensor can be derived from a fitting procedure.[18] Unfortunately, since the degrees of freedom of the hyperpolarizability tensor are more numerous than the experimental constraints, the system remains underdetermined.[18]

Furthermore, the hypothesis of a single averaged hyperpolarizability tensor for all non linear sources is not straightforward for liquid water. Indeed, the solvation shell around each molecule creates an electrostatic field, which strongly perturbs the water first hyperpolarizability.[28,29] Moreover, the perturbation is different for each molecule,[22,30] leading to large fluctuations of the individual molecular responses. However, such local hyperpolarizability fluctuations have been mostly neglected in the interpretation of SHS signals of pure liquid so far. Their presence has been discussed in specific cases,[11,22,31,32] but their impact on the signal were difficult to quantify.

To gain insight in the interpretation of SHS intensities of liquids at the molecular level, we performed Molecular Mechanics/Quantum Mechanical (QM/MM) calculations on liquid water. These provide a quantitative description of both the orientations of water molecules and their individual hyperpolarizabilites. We explored the signature of molecular hyperpolarizability variations in the SHS intensities of liquid water, distinguishing between the incoherent contributions, and short-range coherent contributions. We spotlight that taking into account the hyperpolarizability fluctuations is crucial to reproduce without fitting parameters our experimental polarization-resolved SHS results.

Second Harmonic Generation process involves the conversion of two photons at the fundamental frequency ω into one photon at the harmonic frequency 2ω. It is forbidden, within the dipole approximation, in centro-symmetric media such as liquids. Despite this symmetry, when a high-power laser beam is focused in a homogeneous and isotropic liquid, the local fluctuations that exist on the time scale of the laser pulse, either in the orientations or in the geometries of the molecules, give rise to a scattered intensity at the harmonic frequency. Briefly, the SHS experiment, schematized in Fig. 1(a), consists in illuminating a quartz cell filled by ultra-pure water with a femtosecond laser at wavelength 800 nm. The harmonic photons emitted at 90° relative to the excitation direction are collected, while the polarization angle γ of the fundamental linearly polarized beam is rotated from 0 to 360°. Here, the direction of the exciting laser beam defines the Z-axis, $\gamma = 0°$ corresponds

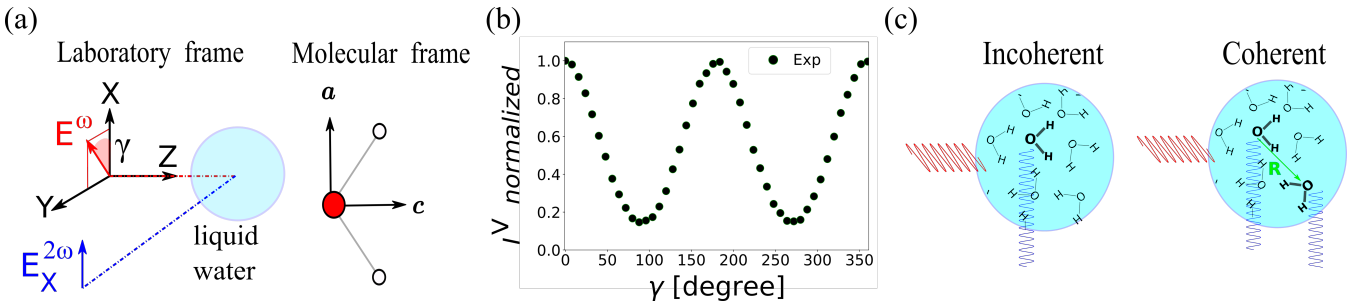

Figure 1: (a) Scheme of the right angle Second Harmonic Scattering (SHS) experiment on liquid water with the definition of the laboratory (X,Y,Z) and molecular (a,b,c) frames. (b) SHS Intensity collected experimentally in V-polarization (along X-axis) I^V as a function of the fundamental polarization angle γ, normalized by $I^V(\gamma = 0)$. (c) Schematic views of the coherent and incoherent contributions to the SHS scattering.

to a vertical polarization along the X-axis, and $\gamma = 90°$ to a horizontal polarization along the Y-axis. The SHS intensity is recorded along the vertical X-axis output polarization direction, providing the $I^V(\gamma)$ polarization plot (see Sect. S1 for further experimental details). Finally, the polarization-resolved curves are normalized by their maximum intensity. In the case of pure water, we obtain the polarization plot of Fig. 1(b) that shows an oscillation that can be described using:[6]

$$I^V(\gamma) = FNI^0\left(\cos^4\gamma + A\cos^2\gamma\sin^2\gamma + D\sin^4\gamma\right), \quad (1)$$

where N is the number of molecules in the scattering volume and F is a constant prefactor including experimental parameters. I^0 is proportional to the SHS intensity emitted per molecule at $\gamma = 0$ and I^0D to the value at $\gamma = 90°$. D is known as the depolarization ratio and is often linked to the molecular symmetries.[7,33,34] The value extracted from our experimental measurements is $D = 0.14\pm0.01$, in agreement with previous results.[10] The intensity I^V is linked to the molecular responses β through the coefficients I^0, A, and D that are proportional to different components of the tensor $\mathcal{Y}$ defined as[6,18,35]

$$\mathcal{Y}_{IJK,RST} = \overbrace{\sum_n \beta^{L,n}_{IJK}\beta^{L,n}_{RST}}^{incoherent} + \overbrace{\sum_{n\neq m} \beta^{L,n}_{IJK}\beta^{L,m}_{RST}}^{coherent} \quad (2)$$

where $\beta^{L,n}$ is the first hyperpolarizability of the molecule number n expressed in the laboratory frame and where I, J, K represent the laboratory axes X, Y or Z (see Sect. S2). One recognizes in Eq. 2 the usual separation into incoherent and coherent contributions:[6] the incoherent one corresponds to the sum of the intensities scattered by each individual molecule of the liquid characterized by its first molecular hyperpolarizability tensor (β), while the coherent one corresponds to the intensities emerging from interferences of responses from different molecules, as illustrated in Fig. 1.(c). Here, the coherent term does not contain any phase factor. Indeed, at optical wavelength and for our QM/MM scheme that takes into account only correlations up to about 1 nm, it can be neglected. Since the proportionality factor F is not measured experimentally and is common to all incoming polarization directions, we will rather discuss the coefficients I^0, A and D or similarly $\mathcal{Y}/N$. Using the definition of the laboratory frame $\{X, Y, Z\}$ presented in Fig. 1.(a), NI^0 is the component $\mathcal{Y}_{XXX,XXX}$ and NI^0D is $\mathcal{Y}_{XYY,XYY}$ (see Sect. S2). In particular, the dimensionless depolarization ratio $D = \mathcal{Y}_{XYY,XYY}/\mathcal{Y}_{XXX,XXX}$ can be measured experimentally and compared to the one obtained by numerical calculations.

In the following, we discuss the different contributions to the intensity via the components of the tensor $\mathcal{Y}/N$. To estimate them, the ensemble of hyperpolarizabilities of all the molecules $\{\beta^n\}_{n\in[1,N]}$ has been calculated using a quantum mechanics (QM)/molecular mechanics (MM) approach. Methological details

are provided in Sect. S3.1. Briefly, in a first step, the structure of the liquid water has been obtained from a classical MD simulation of about 15600 water molecules in their liquid phase in a cubic box, representing a volume of about $(7.8\ \mathrm{nm})^3$. Simulations were performed with the LAMMPS code using the rigid TIP4P/2005 water model. The second step consists in computing, for several MD snapshots, the first molecular hyperpolarizability $\beta^n(2\omega,\omega,\omega)$ of each water molecule using an electrostatic embedding. The hyperpolarisability tensor expressed in the molecular frame of the molecule n, noted $\beta^{M,n}$, depends on the local electrostatic embedding. For each molecule, $\beta^{L,n}$ can be calculated from $\beta^{M,n}$ through the transformation matrice $\mathbf{T}^n$ describing the orientation of the molecule n in the laboratory frame (see Eq. S4). Provided with the ensembles of hyperpolarizabilities $\left\{\beta^{L,n}\right\}_{n\in[1,N]}$ at different times, the tensor $\mathcal{Y}/N$ has been computed, and was finally averaged over several timesteps.

To quantify the impact of molecular hyperpolarizability fluctuations and the weights of each contribution on the SHS intensity, we compared the different values of I^0 and D obtained using four approximations for Eq. 2: taking into account or not the coherent contributions, and taking into account or not the fluctuations of β^M. The comparison between the experimental and calculated depolarization ratio D is particularly relevant because it allows a direct comparison between numerical data and measurements.

Let us first examine the ensemble of hyperpolarizabilities obtained by the QM/MM calculations. In the molecular frame, the different components all strongly fluctuate,[22,30] and their distributions are well described by Gaussian curves (see Figs. S6 and S7). Their mean values $\langle\beta^M\rangle$ and standard deviations $\sigma(\beta^M)$ are summarized in Table 1, where the brackets $\langle\cdot\rangle$ represent the average on all the N molecules, i.e. $\langle\beta\rangle=\sum_n\beta^{M,n}/N$, and the exponent M recalls that one describes the hyperpolarizability in the molecular frame.

As pointed out previously,[22,30] the molecular C_{2v} symmetry is well respected in average and the standard deviations of hyperpolarizability

Table 1: Average and standard deviation of the first hyperpolarizability tensor β^M of water molecules in liquid water, expressed in the molecular frame (see Fig. 1.(a)). The values are calculated for an excitation wavelength of 800 nm, in atomic units, using a QM/MM approach. Standard errors of the means calculated from the dispersion of the 10 values obtained at different timesteps are less than 0.02 a.u.

	caa	*aca*	*cbb*	*bcb*	*ccc*
$\langle\beta^M\rangle$	-1.9	-2.0	2.6	2.3	4.1
$\sigma(\beta^M)$	1.6	1.6	2.9	3.0	4.6

	aaa	*bbb*	*abb*	*abc*
$\langle\beta^M\rangle$	0	0	0	0
$\sigma(\beta^M)$	2.3	9.1	2.6	1.4

are large relative to the mean values. This is especially striking for β_{bbb}, where b is the direction normal to the molecular plane. Its average cancels out because of the molecular C_{2v} symmetry, but its standard deviation is as high as 9.1 a.u. Noticeably, the relationships between β^M components imposed by intrinsic and Kleinman symmetries are well recovered even at optical frequency (see Fig. S6). Concerning the hyperpolarizabilities in the laboratory frame, β^L, all components should cancel out on average because liquid water is isotropic. In the QM/MM results, they indeed all vanish within the error (about 0.1 a.u., see Table S1). This demonstrates that the orientational sampling is satisfactory in our MD simulations.

Rather than the averages of the hyperpolarizability components $\langle\beta^{L,n}_{IJK}\rangle$, the average of their products are relevant to the SHS intensity. We therefore calculated the averages of $(\beta^{L,n}_{XXX})^2$ and $(\beta^{L,n}_{XYY})^2$ emerging from the QM/MM approach and we compare these values to the analytical expressions established when the absolute molecular orientations and β^M hyperpolar-

izabilities are uncorrelated:[7,33]

$$\left\langle \left(\beta^{L,n}_{XXX}\right)^2 \right\rangle = \frac{1}{105}\Big\langle \sum_{ijk} 2(\beta^{M,n}_{ijk})^2 + \beta^{M,n}_{ijj}\beta^{M,n}_{ikk} + 4\beta^{M,n}_{iij}\beta^{M,n}_{jkk} + 4\beta^{M,n}_{iij}\beta^{M,n}_{kkj} + 4\beta^{M,n}_{ijk}\beta^{M,n}_{jki} \Big\rangle, \quad (3)$$

$$\left\langle \left(\beta^{L,n}_{XYY}\right)^2 \right\rangle = \frac{1}{105}\Big\langle \sum_{ijk} 6(\beta^{M,n}_{ijk})^2 + 3\beta^{M,n}_{ijj}\beta^{M,n}_{ikk} - 2\beta^{M,n}_{iij}\beta^{M,n}_{jkk} - 2\beta^{M,n}_{iij}\beta^{M,n}_{kkj} - 2\beta^{M,n}_{ijk}\beta^{M,n}_{jki} \Big\rangle, \quad (4)$$

where i, j, k runs on the molecular axes a, b, c and the brackets represent the averaging on all the molecules [1]. It turns out that Eqs. 3 and 4 are fulfilled by our QM/MM data with relative errors lower than 1%. In the following, we shall exploit these relationships to quantify the importance of the fluctuations of the β^M components on the SHS intensity.

We then investigate the incoherent contribution to the SHS intensity. To do so, the second sum of Eq. 2 has been neglected. The incoherent contribution contains solely the squared hyperpolarizabilities expressed in the laboratory frames, $\langle(\beta^{L,n}_{IJK})^2\rangle$. Thus, $I^0 = \langle(\beta^{L,n}_{XXX})^2\rangle$ and $D = \langle(\beta^{L,n}_{XYY})^2\rangle / \langle(\beta^{L,n}_{XXX})^2\rangle$. To quantify the importance of the fluctuations of β^M, we compare the polarization-resolved SHS intensity curves obtained in two cases depicted in Fig. 2(a) : either the hyperpolarizability tensor is the same for all molecules, and is equal to the average value $\langle\beta^M\rangle$, or the fluctuations of the QM/MM data set is included. For the first case, inserting the calculated $\langle\beta^M\rangle$ components from Table 1 into the r.h.s. of Eqs. 3 and 4 yields $I^0 = 4.3$ a.u. and $D = 0.384$ and a polarization curve represented by the dashed red line on Fig. 2.(b). In that case, D is more than twice the experimental value. By contrast, when the fluctuations of β^M are taken into account, the scattering intensity I^0 increases to a value of $I^0 = 38.2$ a.u., almost 10 times the

[1] These general expressions are usually simplified by taking into account molecular symmetries, or Kleinman symmetries [6,33,36]

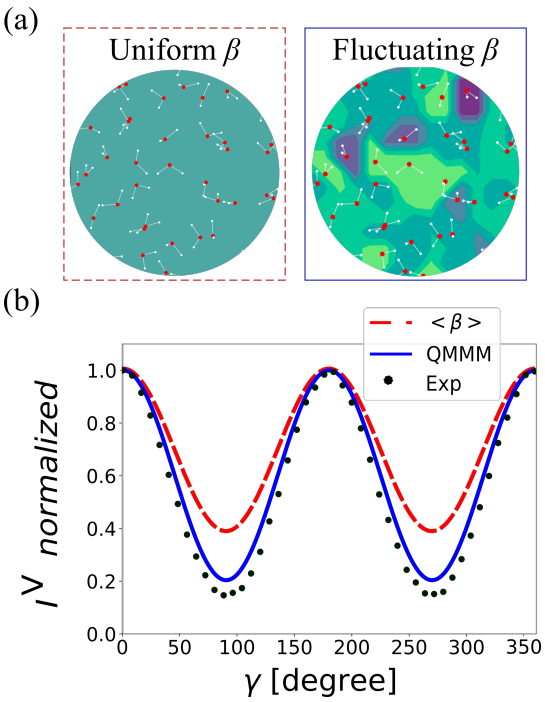

Figure 2: (a) Illustration of the two hypotheses made on the hyperpolarizability tensor β^M. Left: same tensor for all molecules. Right: each molecule has its own tensor, obtained by QM/MM calculation. (b) Collected harmonic intensity I^V as a function of the input-polarization angle γ. The data obtained experimentally (dots) are compared to the numerical results in the incoherent limit, either with a fixed hyperpolarizability (dashed red line) or with the fluctuating hyperpolarizabilities obtained by QM/MM (solid blue line).

former one. As Eqs. 3 and 4 recall, both the fluctuations of the individual components of β^M and the correlations between its different components contribute to the incoherent scattering intensity (see Sect. S4.3 for more details). Noticeably, including fluctuations decreases D to 0.204. This value is closer to the experimental value, as illustrated by the polarization curve represented by a blue solid line on Fig. 2.(b). Yet, it does not match the experimental data. The incoherent contributions alone thus fail to reproduce the experimental SHS depolarization ratio.

Finally, we also consider the coherent contributions described by the second term of $\mathcal{Y}$ in Eq. 2. Tocci et al. have shown that oriental correlations in the first solvation shell can

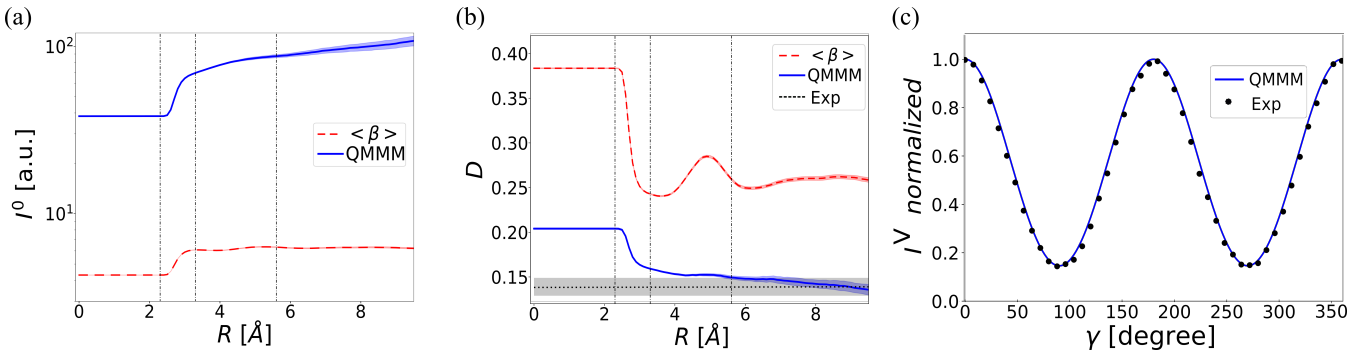

Figure 3: (a) Evolution of the amplitude of SHS scattering intensity and (b) of the depolarization ratio D with the distance R up to which the hyperpolarizability correlations are taken into account, either for a constant average hyperpolarizability (red) or with individual hyperpolarizability obtain by QM/MM calculation (blue). The vertical dotted lines represent the limits between the solvation layers, defined from the peaks of the pair correlation function, see Fig. S1. The experimental depolarization ratio is represented by the black dotted curve. The colored shadows around the solid curves represent the error bars (see Sect. S3.2.4). (c) Comparison of the experimental normalized SHS intensity $I^V/I^V(\gamma = 0)$, represented by dots, with the one obtained with QM/MM modeling, including both the incoherent and coherent contributions up to $R = 7$ Å .

modify the SHS intensity.[18] However, they assumed a constant "effective" hyperpolarizabilty that has to be fitted to recover the experimental data. Here, we did not use a fitted hyperpolarizability, but the individual values obtained by QM/MM to calculate $\mathcal{Y}/N$.

Since the orientational and hyperpolarizability correlations are expected to decrease when molecules are further apart, we quantify the effect of the coherent contributions as a function of the distance R between the pairs of molecules. To do so, we evaluate

$$\frac{\mathcal{Y}(R)}{N} = \frac{1}{N} \sum_{R^{mn} \leq R} \beta^{L,n} \beta^{L,m}, \qquad (5)$$

where the summation includes solely pairs of molecules $\{m, n\}$ that are closer than the distance R, i.e. the intermolecular distance R^{mn} is smaller or equal to R. This partial summation yields an intensity $I^0(R)$ and a depolarization ratio $D(R)$ presented in Figs. 3.(a) and (b) respectively (see Sect. S3.2 for details). When $R = 0$, we recover the values corresponding to the incoherent contributions presented previously. When R increases, ie when the coherent terms are progressively included, the intensity increases whereas the depolarization ratio decreases. Their variations are strong in the first solvation layer, smaller in the second layer and even smaller in the third layer. For R larger than about 7 Å , the signal-to-noise ratio becomes low (see Fig. S5). Therefore, we discuss here the values of $I^0(R)$ and $D(R)$ integrated up to $R \simeq 7$Å . They are compared to the values obtained for $R = 0$ – corresponding to the incoherent contributions only – in Table 2.

Table 2: Comparison of intensity I^0 and depolarization ratio D of the SHS intensity I^V when different terms are taken into account (see text for details). I^0 is expressed in atomic unit for β, squared.

Incoh.	β^M fluct.	Coh.	I^0	D
✓	✗	✗	4.3	0.38
✓	✗	✓	6.2	0.26
✓	✓	✗	38.2	0.20
✓	✓	✓	94.4	0.14
	Experimental value			0.14

Concerning the intensities, in Fig. 3.(a), the logarithmic scale permits to compare the effect of the coherent contributions using either the averaged hyperpolarizability tensor $\langle \beta^M \rangle$ (dashed red curve) or the fluctuating QM/MM one (solid blue curve) : the tendencies are qualitatively similar but the coherent contri-

bution is stronger when β^M fluctuations are present. There are not only orientational correlations, but also correlations among the molecular hyperpolarizability tensors. Concerning the depolarization ratios (see Fig. 3.(b)), the one predicted by QM/MM for liquid water is $D(7\text{Å}) = 0.145 \pm 0.004$, very close to the experimental value $D^{exp} = 0.14 \pm 0.01$ (gray area). In contrast, considering the coherent terms in $\mathcal{Y}$ without the β^M fluctuations fails to predict an accurate depolarisation ratio. Table 2 recalls the intensities and depolarization ratios obtained taking into account or not the fluctuations of β^M, and taking into account or not the coherent contributions. An accurate depolarization ratio can only be obtained by including both the short-range coherent contributions, and the fluctuations of the hyperpolarizability β^M.

Finally, concerning the polarization plots of the SHS intensity, our QM/MM calculations are in very good agreement with the experimental data, without any adjustable parameters, see Fig. 3.(c), even if our approach does not describe orientation correlations at distances larger than about 1 nm.

To conclude, the SHS intensity of liquid water has been modeled by using QM/MM calculations that provides the dipolar hyperpolarizabilities of individual molecules embedded in a liquid environment. Both coherent and incoherent contributions to the SHS intensity are significant. First, it has been shown that the incoherent part increases by almost one order of magnitude thanks to the hyperpolarizability fluctuations, which are strong in liquid water. Second, the coherent contributions due to the short-range correlations between intermolecular responses have been investigated in details. The orientational correlations in the first solvation shells are accompanied by hyperpolarizability correlations that modulate the SHS intensity. We notably reproduce for the first time the depolarization ratio of pure liquid water without any adjustable parameters. The long-range orientational correlations are not included in our approach, but they may be included to model the intensity in even finer details, that are beyond the present study.

Our QM/MM approach will now be developed to study the SHS signal of other solvents or aqueous solutions. We hope our results will help to complete the interpretation of Second Harmonic Scattering experiments of molecular liquids.

Acknowledgement The authors acknowledge useful discussions with P.-F. Brevet, J. Duboisset, R. Everaers and L. Joly. They also gratefully acknowledge support from the PSMN (Pôle Scientifique de Modélisation Numérique) of the ENS de Lyon for the computing resources. OB thanks the financial support of the French National Agency for Research under project Solstice (ANR-21-CE30-0007). EB thanks the financial support of the French National Agency for Research under project Profile (ANR-17-CE29-0009)

Supporting Information Available

Experimental details on polarization-resolved SHS intensities. Summary of the SHS formalism. Methodological details (QM/MM Method, Numerical analysis of hyperpolarizability correlations). Details on Results (First hyperpolarizability in the molecular frame, First hyperpolarizability in the laboratory frame, Details of the contributions of fluctuations or correlations to the incoherent part of the tensor $\mathcal{Y}$.)

References

(1) Nandi, N.; Bhattacharyya, K.; Bagchi, B. Dielectric Relaxation and Solvation Dynamics of Water in Complex Chemical and Biological Systems. Chemical Reviews **2000**, 100, 2013–2046, PMID: 11749282.

(2) Bocquet, L. Nanofluidics coming of age. Nature Materials **2020**, 19, 254–256.

(3) Belorizky, E.; Fries, P. H.; Guillermo, A.; Poncelet, O. Almost ideal 1d water diffusion in imogolite nanotubes evidenced by NMR relaxometry. ChemPhysChem **2010**, 11, 2021–2026.

(4) Fournier, J. A.; Carpenter, W.; De Marco, L.; Tokmakoff, A. Interplay of Ion–Water and Water–Water Interactions within the Hydration Shells of Nitrate and Carbonate Directly Probed with 2D IR Spectroscopy. Journal of the American Chemical Society **2016**, 138, 9634–9645, PMID: 27404015.

(5) Zhang, C.; Yue, S.; Panagiotopoulos, A. Z.; Klein, M. L.; Wu, X. Dissolving salt is not equivalent to applying a pressure on water. Nature Communications **2022**, 13, 8–13.

(6) Bersohn, R.; Yoh-Han, P. A.; Frisch, H. L. Double-quantum light scattering by molecules. The Journal of Chemical Physics **1966**, 45, 3184–3198.

(7) Brasselet, S.; Zyss, J. Multipolar molecules and multipolar fields: probing and controlling the tensorial nature of nonlinear molecular media. Journal of the Optical Society of America B **1998**, 15, 257–288.

(8) Shelton, D. P. Collective molecular rotation in D2O. Journal of Chemical Physics **2002**, 117, 9374–9382.

(9) Rodriguez, V.; Grondin, J.; Adamietz, F.; Danten, Y. Local structure in ionic liquids investigated by hyper-Rayleigh scattering. Journal of Physical Chemistry B **2010**, 114, 15057–15065.

(10) Shelton, D. P. Long-range orientation correlation in water. The Journal of Chemical Physics **2014**, 141, 224506.

(11) Rodriquez, M. B.; Shelton, D. P. What is measured by hyper-Rayleigh scattering from a liquid? Journal of Chemical Physics **2018**, 148.

(12) Pardon, A.; Bonhomme, O.; Gaillard, C.; Brevet, P. F.; Benichou, E. Nonlinear optical signature of nanostructural transition in ionic liquids. Journal of Molecular Liquids **2021**, 322.

(13) Smolentsev, N.; Roke, S. Self-Assembly at Water Nanodroplet Interfaces Quantified with Nonlinear Light Scattering. Langmuir **2020**, 36, 9317–9322, PMID: 32654491.

(14) Bonhomme, O.; Sanchez, L.; Benichou, E.; Brevet, P. Multistep Micellization of Standard Surfactants Evidenced by Second Harmonic Scattering. The Journal of Physical Chemistry B **2021**, 125, 10876–10881.

(15) Chen, Y.; Dupertuis, N.; Okur, H. I.; Roke, S. Temperature dependence of water-water and ion-water correlations in bulk water and electrolyte solutions probed by femtosecond elastic second harmonic scattering. Journal of Chemical Physics **2018**, 148.

(16) Belloni, L.; Borgis, D.; Levesque, M. Screened Coulombic Orientational Correlations in Dilute Aqueous Electrolytes. The Journal of Physical Chemistry Letters **2018**, 9, 1985–1989, PMID: 29543464.

(17) Duboisset, J.; Rondepierre, F.; Brevet, P. F. Long-Range Orientational Organization of Dipolar and Steric Liquids. Journal of Physical Chemistry Letters **2020**, 11, 9869–9875.

(18) Tocci, G.; Liang, C.; Wilkins, D. M.; Roke, S.; Ceriotti, M. Second-harmonic scattering as a probe of structural correlations in liquids. The Journal of Physical Chemistry Letters **2016**, 7, 4311–4316.

(19) Borgis, D.; Belloni, L.; Levesque, M. What Does Second-Harmonic Scattering Measure in Diluted Electrolytes? The Journal of Physical Chemistry Letters **2018**, 9, 3698–3702.

(20) Shelton, D. P. Long-range orientation correlation in dipolar liquids probed by hyper-Rayleigh scattering. Journal of Chemical Physics **2015**, 143, 1–6.

(21) Shelton, D. P. Structural correlation in water probed by hyper-Rayleigh scattering. Journal of Chemical Physics **2017**, 147, 1–8.

(22) Liang, C.; Tocci, G.; Wilkins, D. M.; Grisafi, A.; Roke, S.; Ceriotti, M. Solvent fluctuations and nuclear quantum effects modulate the molecular hyperpolarizability of water. Physical Review B **2017**, 96, 1–6.

(23) Duboisset, J.; Brevet, P. F. Salt-induced Long-to-Short Range Orientational Transition in Water. Physical Review Letters **2018**, 120, 263001.

(24) Gassin, P.-M.; Prelot, B.; Gregoire, B.; Martin-Gassin, G. Second-Harmonic Scattering Can Probe Hydration and Specific Ion Effects in Clay Particles. The Journal of Physical Chemistry C **2020**, 124, 4109–4113.

(25) Martin-Gassin, G.; Paineau, E.; Launois, P.; Gassin, P.-M. Water Organization around Inorganic Nanotubes in Suspension Probed by Polarization-Resolved Second Harmonic Scattering. The Journal of Physical Chemistry Letters **2022**, 13, 6883–6888, PMID: 35862242.

(26) Dupertuis, N.; Tarun, O. B.; Lütgebaucks, C.; Roke, S. Three-Dimensional Confinement of Water: H2O Exhibits Long-Range (¿50 nm) Structure while D2O Does Not. Nano Letters **2022**, 22, 7394–7400, PMID: 36067223.

(27) Roesel, D.; Eremchev, M.; Schönfeldová, T.; Lee, S.; Roke, S. Water as a contrast agent to quantify surface chemistry and physics using second harmonic scattering and imaging: A perspective. Applied Physics Letters **2022**, 120, 160501.

(28) Mikkelsen, K. V.; Luo, Y.; Ågren, H.; Jørgensen, P. Sign change of hyperpolarizabilities of solvated water. The Journal of Chemical Physics **1995**, 102, 9362–9367.

(29) Sylvester-hvid, K. O.; Mikkelsen, K. V.; Norman, P.; Jonsson, D.; Agren, H. Sign Change of Hyperpolarizabilities of Solvated Water, Revised: Effects of Equilibrium and Nonequilibrium Solvation. J. Phys. Chem. A **2004**, 108, 8961–8965.

(30) Le Breton, G.; Bonhomme, O.; Brevet, P.-F.; Benichou, E.; Loison, C. First hyperpolarizability of water at the air–vapor interface: a QM/MM study questions standard experimental approximations. Phys. Chem. Chem. Phys. **2021**, 23, 24932–24941.

(31) Loison, C.; Nasir, M. N.; Benichou, E.; Besson, F.; Brevet, P.-F. Multi-scale modeling of mycosubtilin lipopeptides at the air/water interface: structure and optical second harmonic generation. Phys. Chem. Chem. Phys. **2014**, 16, 2136–2148.

(32) Bouquiaux, C.; Tonnelé, C.; Castet, F.; Champagne, B. Second-Order Nonlinear Optical Properties of an Amphiphilic Dye Embedded in a Lipid Bilayer. A Combined Molecular Dynamics–Quantum Chemistry Study. The Journal of Physical Chemistry B **2020**, 124, 2101–2109, PMID: 32105079.

(33) Castet, F.; Bogdan, E.; Plaquet, A.; Ducasse, L.; Champagne, B.; Rodriguez, V. Reference molecules for nonlinear optics: A joint experimental and theoretical investigation. Journal of Chemical Physics **2012**, 136.

(34) Heesink, G. J. T.; Ruiter, A. G. T.; van Hulst, N. F.; O lger, B. Determination of hyperpolarizability tensor components by depolarized hyper Rayleigh scattering. Physical Review Letters **1993**, 71, 999.

(35) Chen, Y.; Roke, S. Generalized expressions for hyper-Rayleigh scattering from isotropic liquids. 2017; `https://arxiv.org/abs/1705.04231`.

(36) De Wergifosse, M.; Castet, F.; Champagne, B. Frequency dispersion of the

first hyperpolarizabilities of reference molecules for nonlinear optics. Journal of Chemical Physics **2015**, 142.